

**Theoretical Advances in Current Estimation and Navigation from a
Glider-Based Acoustic Doppler Current Profiler (ADCP)**

Jacob Stevens-Haas^a, Sarah E. Webster^b, Aleksandr Aravkin^a

^a*Department of Applied Mathematics, University of Washington.* ^b*Applied Physics Laboratory,
University of Washington*

arXiv:2110.10199v1 [math.OC] 19 Oct 2021

Corresponding author: Jacob Stevens-Haas, jmsh@uw.edu

ABSTRACT: We examine acoustic Doppler current profiler (ADCP) measurements from underwater gliders to determine glider position, glider velocity, and subsurface current. ADCPs, however, do not directly observe the quantities of interest; instead, they measure the relative motion of the vehicle and the water column. We examine the lineage of mathematical innovations that have previously been applied to this problem, discovering an unstated but incorrect assumption of independence. We reframe a recent method to form a joint probability model of current and vehicle navigation, which allows us to correct this assumption and extend the classic Kalman smoothing method. Detailed simulations affirm the efficacy of our approach for computing estimates and their uncertainty. The joint model developed here sets the stage for future work to incorporate constraints, range measurements, and robust statistical modeling.

SIGNIFICANCE STATEMENT: The trade-offs between cost, power, and mission duration of ocean gliders allow them to measure underwater currents around the world. We seek to improve the methods used by seagliders to infer true current profiles and vehicle position from limited data. Where previous methods applied smoothing techniques ad hoc, we start with a probability model for current and navigation from which we derive a more powerful and flexible smoothing method. In simulation, our method performed well, able to track within 75m a vehicle submerged and without GPS for three hours. The flexible method allows experimenting with innovations from recent robust process model literature, including more difficult range measurements, and potentially real-time processing by low-powered gliders.

1. Introduction

In order to map subsurface currents far away from fixed and mobile infrastructure, underwater gliders embark small, 1 MHz acoustic Doppler current profilers (ADCP). These high-resolution profilers, when embarked on a vehicle such as a seaglider, measure the relative velocity of the water column. Using these measurements poses a challenge because they reference the vehicle's navigation frame and only sample a local slice of the water column. Nevertheless, one can use these relative velocities together with surface GPS measurements and a set of useful assumptions, to separate the relative measurement into its ground-referenced components: the subsurface ocean current profile and vessel navigation velocity. Doing so eliminates the reliance on navigation support from acoustic long baseline beacons or surface tenders, as in Jakuba et al. (2021).

Previous efforts to develop a method for inferring currents and navigational data from ADCP measurements began with low-resolution sensors that imaged the entire water column. The sensors typically descended from either a ship or fixed mooring. Higher-resolution profilers had a limited range, and thus Firing and Gordon (1990) developed a "shear" method to stitch together frames: the change in ADCP returns are averaged across overlapping depths to form the baroclinic part of the current profile.

Visbeck (2002) developed what is now the most widely used method, a linear least squares model commonly referred to as the "inversion" method. The inversion method originally involved one step to measure depth-averaged current (DAC) and another to solve the matrix inverse problem.

Methods derived from Visbeck (2002) differ according to whether smoothing occurs through a process-model or through a finite difference regularizer; whether the model includes other sensors such as bottom-tracking Doppler velocity log, inertial sensors, or terrain matching; whether the model treats currents as horizontally and temporally stable; and what measurement errors, such as sensor misalignment and ADCP bias, the method seeks to control. The particulars of each method often reflect whether it aims to support seaglidors or propeller-driven AUVs. Medagoda et al. (2016) contains a literature review of both corpora, while we focus more specifically on the former.¹

Contributions and roadmap.

We present an improved inversion method based on Jonker et al. (2019), which frames the combined smoothing/ADCP inverse problem as a single joint optimization problem.² We start a step further back, with the stochastic model that gives rise to the physical problem. The more theoretical starting point allows us to compute the proper smoothing covariance between the current and the vehicle's over-the-ground velocity and position. We then derive the joint optimization problem from the posterior mode of vehicle and current states. The approach utilizes ADCP data, hydrodynamic model data, and GPS location fixes (at the start and, optionally, at the end of the dive). We demonstrate the success of the method in simulations without either a final GPS point, Doppler Velocity Log (DVL) seabed measurements, or IMU measurements.

The paper proceeds as follows. We illustrate connections to relevant prior work in Section 2. Section 3 describes the state-space model for our method, including the details of covariance calculations between current and vehicle velocity. It then describes the measurements we include in our model, assembles the final optimization model variants, and finishes with a discussion of uncertainty quantification. Section 4 describes our simulations, numerical experiments, and results. We conclude with a discussion and outline future work.

¹The more complex methods generally aim to satisfy the needs of propeller-driven vehicles. Such vehicles often conduct missions more concerned with precise navigation than current field modeling. The methods also incorporate sensors that require more power and space than available on a typical underwater glider, such as the tactical-grade IMU of Medagoda et al. (2010).

Beyond the review in Medagoda et al. (2016), valuable AUV-focused contributions have occurred in Arnold and Medagoda (2018) and Medagoda and Kinsey (2016), which test out different filters, a physics-based model, and Liu et al. (2021) which suggests a circular calibration dive prior to mission start and a high-pass filter in order to control IMU biases.

²In the above taxonomy, their method, designed for seaglidors, uses a process model smoother, minimal additional sensors, and a one-dimensional current field.

2. Comparison with Prior Methodologies

We begin this section with an explanation of the inversion method in Visbeck (2002), focusing on elements that this paper’s antecedents have improved. The basic method centers on the linear equation:

$$\mathbf{b} = \mathbf{A}\mathbf{x}$$

where the vector \mathbf{b} contains the set of ADCP measurements. The state vector, \mathbf{x} , represents the desired information as a stacked vector:

$$\mathbf{x} := \begin{bmatrix} \mathbf{x}_v \\ \mathbf{x}_c \end{bmatrix},$$

with \mathbf{x}_v as the vehicle velocity at different times and \mathbf{x}_c as the true ocean currents at different depths. The measurement matrix, \mathbf{A} , selects the appropriate depth of current and time of vehicle motion for each ADCP measurement of relative velocity. Binning the state vector makes the system overdetermined, and we can solve it using least squares:

$$\mathbf{x} = (\mathbf{A}^T \mathbf{A})^{-1} \mathbf{A}^T \mathbf{b}.$$

In the absence of binning, an acceptable condition number of $\mathbf{A}^T \mathbf{A}$ requires additional measurement or smoothing terms.³

Although Visbeck (2002) bins the state vector, the paper still offers a smoothing term for currents and two additional, mutually-exclusive measurement terms. The first additional measurement term, that paper’s expression (26), regularizes the depth-average of current (DAC), or barotropic current, to be zero. Thus, the regularizer implicitly changes \mathbf{x}_c to model just *baroclinic* currents and shifts \mathbf{x}_v by DAC. The paper then suggests that DAC or surface current could be calculated separately and added in to correct these values. On the other hand, the alternative expression (30) in Visbeck (2002) forces the integral of vehicle velocities to be equal to the displacement of the vehicle, as

³Without binning, the system would be underdetermined. \mathbf{x} would have two entries for each entry of \mathbf{b} , because there is both a vehicle velocity and a current to infer at each measurement point.

measured by GPS. Such a term obviously requires \mathbf{x}_v represent true, over-the-ground velocity and \mathbf{x}_c represent the true current.

Todd et al. (2017) identifies that the DAC regularization, expression 26 of Visbeck (2002), can act instead as a measurement term if one calculates DAC before the inversion method. He calculates the DAC “measurement” from the difference between GPS measurement and dead reckoning, where a hydrodynamic model supplies dead reckoning. In addition, to correct the hydrodynamic model, the work describes a method to pre-calculate ADCP misalignment, pitch error biases, angle of attack, and sideslip. Thus, while following the method of expression 26, Todd’s two-step method still models vehicle over-the-ground velocity. Although the reconciled DAC expression nominally would allow a GPS displacement measurement term like expression (30) of Visbeck (2002), the method already expends the GPS-measured displacement in calculating DAC. It does, however, include a GPS-derived surface velocity measurement. Finally, both Todd et al. (2011) and Todd et al. (2017) smooth, not just the current velocity as in Visbeck (2002), but the vehicle velocity as well.

Jonker et al. (2019) reflect that one need not compose all the hydrodynamic model terms and GPS displacement into a single measurement of depth-averaged current; these terms may factor more properly as individual measurements in a combined model. Indeed, Visbeck (2002) advocates the ease with which least squares models can accommodate additional measurements. However, as we point out, that ease of adding terms relies on their putative independence as much as it relies on the linear nature of the problem formulation.⁴ The paper’s second combined model smooths currents and vehicle process using a Kalman smoother, replacing the finite difference smoothing of Visbeck (2002), Todd et al. (2011), and Todd et al. (2017). The smoother requires modeling both the vehicle horizontal position as well as velocity, which simplifies the GPS measurement term. Such a process model approach has prior exploration in Medagoda et al. (2010) and follow-on papers.⁵ These papers use an inversion approach and focus on propeller-driven AUVs with an IMU in shallower water. Their process model filter, in distinction to a smoother, calculates the optimal value from recent, real-time observations, as opposed to the greater power but greater expense of retaining the entire state history, as in the smoother of Jonker et al. (2019). As a final note, Jonker et al. (2019)

⁴Easy incorporation of measurements faces additional drawbacks; Jonker et al. (2019)’s error modeling cannot accommodate all the innovation in error modeling of Todd et al. (2017) without process terms for the sideslip and angle-of-attack errors.

⁵Medagoda and co-authors test out a variety of filters: a Sparse Extended Information Filter in Medagoda et al. (2010), Medagoda et al. (2011a), and Medagoda et al. (2011b), an Extended Kalman Filter in Medagoda et al. (2015), an Extended Information Filter in Medagoda et al. (2016), and an Unscented Kalman Filter in Arnold and Medagoda (2018).

mentions that vehicle smoothing ought to properly apply to vehicle through-the-water velocity, not over-the-ground velocity. However, because such independent smoothing would require modeling through-the-water velocity and consequent difficulties incorporating GPS measurement, Jonker et al. (2019) does not do so.

Overall, we contribute several important improvements to the method. We explicitly model the problem as a maximum likelihood estimator, including process terms for the current and the vehicle kinematics. This probability model lets us derive the correct covariances to smooth the vehicle’s through-the-water velocity while still modeling the vehicle’s over-the-ground velocity. The process model approach also allows us to avoid binning the of data as well as to compare the smoothing of different process models. Finally, viewing the current and vehicle smoothing as a consequence of a stochastic process illuminates several additional assumptions whose refinement could improve the model performance.

3. Methods

Here, we specify the Gaussian current and navigation random processes and sensor measurement error. Then, we combine terms in a single optimization problem for the latent current and vehicle variables and estimate them using maximum likelihood.

a. Process Model

A process model for current and vehicle motion smooths available measurements by applying a prior, or regularizer. We use the vector \mathbf{x} to describe the combined state space of the vehicle and current. The state vector, \mathbf{x} , includes the vehicle’s velocity and position on a local Cartesian grid and the water’s velocity. Moreover, it eschews the need to bin observations: \mathbf{x} has vehicle kinematic entries at every time observed and current entries at every depth observed. We use a subscript to denote when selecting some subset of the state; e.g. \mathbf{x}_v represents just the time-indexed vehicle components of the state (both position and velocity). In implementation, any subscript manifests as matrix multiplication. A complete list of this notation follows:

1. \mathbf{x}_v Vehicle components
2. \mathbf{x}_c Current components
3. \mathbf{x}_q vehicle position components, one part of \mathbf{x}_v

4. $\mathbf{x}_{\dot{g}}$ vehicle velocity components, the other part of \mathbf{x}_v

The method does not account for compass measurements or model heading, leaving such items to preprocessing. Consequently, we can expect an additional 17m of error for every degree of uncorrected compass error and every kilometer traveled. Moreover, without an inertial measurement, we do not have a need for earth curvature terms; a local grid will not supply more than a .1% error over the distances of a single dive between the 45th parallels. As a final note, the assumption that preprocessing handles vehicle and geodetic orientation gives us all measurements in cardinal directions. As such, the northerly and easterly components of our model comprise two non-interacting problems. When we specify a model term, we implicitly mean two terms: one for the northerly component, and one for the easterly component.

In our initial model for $\Pr(\mathbf{x})$, we use a standard Kalman smoother, the maximum likelihood estimator for a particle whose velocity obeys Brownian motion. This probability model gives a negative log-likelihood term of:

$$-\ell(\mathbf{x}_v) = \frac{1}{2\sigma_v^2} \|\mathbf{G}_v \mathbf{x}_v\|_{\mathbf{Q}_v^{-1}}^2, \quad (1)$$

where Appendix A contains details of the update matrix \mathbf{G}_v and covariance matrix \mathbf{Q}_v . A user-defined covariance scaling, σ_v^2 , completes the term.

The current process adds an analogous term, with three distinctions. Firstly, current varies by depth s and not time t . Second, the basic model only requires the water velocity and has no need for a current “position.” Finally, in order to approximate the time/horizontal variance in the water column, we treat ascent as continuing the dive by reflecting depths on ascent across the max depth. This innovation rolls variance due to horizontal, vertical, and time dimensions into a single process. Because of the straight paths that seagliders tend to dive, this reflection should not degrade results significantly. The negative log likelihood contribution for the current process mirrors the one for \mathbf{x}_v :

$$-\ell(\mathbf{x}_c) = \frac{1}{2\sigma_c^2} \|\mathbf{G}_c \mathbf{x}_c\|_{\mathbf{Q}_c^{-1}}^2, \quad (2)$$

where Appendix A contains details of the update matrix \mathbf{G}_c and covariance matrix \mathbf{Q}_c . A user-defined covariance scaling, σ_c^2 , completes the term.

We can compare these terms to the smoothers and regularizers employed in binning methods. If intervals between observations remained constant, our method would regularize the first forwards difference of velocity.⁶ Visbeck (2002) and Todd et al. (2011) instead regularize the 2nd centered difference, which does not have a probabilistic representation in our model.

b. Measurement Terms

In addition to the priors responsible for smoothing the current and vehicle processes, we need measurement terms. We use ADCP measurements of the shear velocity of the water column at one depth and the vehicle over-the-ground velocity at the same time. A hydrodynamic model estimates vehicle through-the-water velocity, mathematically similar to an ADCP measurement, but for which we allow a different error variance. Finally, a pair of GPS fixes either at the beginning of the dive or spanning it measure the change in vehicle position.

We present the measurement error expressions below. \mathbf{B}^q , or $\mathbf{B}^{\dot{q}}$ selects the vehicle kinematics of the state vector at the appropriate measurement times and \mathbf{B}^c selects the currents of the state vector at the appropriate measurement depths. Each term has a user-specified variance parameter σ^2 , representing the measurement error variance; one can set these parameters based on published sensor accuracy. Again, we only give the explicit terms for either the easterly or northerly components; in actuality, we use two of each term.

1. \mathbf{z}_{adcp} : ADCP data measured from the seaglider with error variance σ_{adcp}^2 . This measurement reflects the current at a certain depth relative to the true velocity of the glider:

$$-\ell(\mathbf{z}_{adcp}|\mathbf{x}) = \frac{1}{2\sigma_{adcp}^2} \|\mathbf{z}_{adcp} - (\mathbf{B}_{adcp}^q \mathbf{x}_{\dot{q}} - \mathbf{B}_{adcp}^c \mathbf{x}_c)\|^2. \quad (3)$$

2. \mathbf{z}_{ttw} : Through-the-water estimated velocity of the seaglider with error variance σ_{ttw}^2 . While this quantity nominally relies on calculations from pitch and depth rate measurements using a vehicle's hydrodynamic model, we treat it as direct measurement. It behaves conceptually the same as ADCP data measured at the exact depth of the vehicle.

$$-\ell(\mathbf{z}_{ttw}|\mathbf{x}) = \frac{1}{2\sigma_{ttw}^2} \|\mathbf{z}_{ttw} - (\mathbf{B}_{ttw}^q \mathbf{x}_{\dot{q}} - \mathbf{B}_{ttw}^c \mathbf{x}_c)\|^2. \quad (4)$$

⁶But more rigorously, because the Kalman smoother also includes regularization of vehicle position according to its covariance with velocity.

3. \mathbf{z}_{gps} : GPS position measurements at the surface before and after a dive with error variance σ_{gps}^2 .

$$-\ell(\mathbf{z}_{gps}|\mathbf{x}) = \frac{1}{2\sigma_{gps}^2} \|\mathbf{z}_{gps} - (\mathbf{B}_{gps}^d \mathbf{x}_q)\|^2.$$

These terms compose the complete likelihood specification for the model:

$$-\ell(\mathbf{x}|\mathbf{z}) = -\ell(\mathbf{x}_v) - \ell(\mathbf{x}_c) - \ell(\mathbf{z}_p|\mathbf{x}) - \ell(\mathbf{z}_{itw}|\mathbf{x}) - \ell(\mathbf{z}_{gps}|\mathbf{x}). \quad (5)$$

While other authors model more robust measurement terms, we omit terms for compass error, ADCP bias due to misalignment, or hydrodynamic model bias due to sideslip and angle-of-attack errors aggravated by biofouling.

c. Extensions

Here we discuss the extensions and variations of our basic model.

1) HIGHER-ORDER SMOOTHING.

In Subsection 3.a, we described vehicle over-the-ground velocity and current as Brownian processes. The vehicle's over the ground position then becomes the integral of Brownian motion. Whereas previous authors have described the concomitant regularizer as a smoothing term, strictly speaking, the assumption of Brownian motion implies non-smoothness. We can instead expand our state space model to include higher order terms: vehicle acceleration and the change in current with respect to depth. These terms then become Brownian. Their integrals, vehicle velocity and current velocity, become smooth.

This decision changes the process update matrices, \mathbf{G}_v and \mathbf{G}_c , and the covariance matrices, \mathbf{Q}_v and \mathbf{Q}_c , as described in Appendix B.

Now that our current process has more than one order, we use \mathbf{x}_p to refer specifically to the velocity components of the current process. \mathbf{x}_c then refers more generally to all the current process terms in the same way that \mathbf{x}_v refers to \mathbf{x}_q , \mathbf{x}_j , and now $\mathbf{x}_{\ddot{j}}$

2) INDEPENDENCE.

Unfortunately, our likelihood expression 5 implies an incorrect assumption. Adding together $-\ell(\mathbf{x}_v)$ and $-\ell(\mathbf{x}_c)$ implies that the joint probability $\Pr(\mathbf{x}_v, \mathbf{x}_c) = \Pr(\mathbf{x}_v)\Pr(\mathbf{x}_c)$, which in turn implies independence of the vehicle's over-the-ground velocity from current. Previous authors who modeled over-the-ground vehicle kinematics and additively smoothed both current and vehicle kinematics made the same assumption *de facto*. Instead, the glider's *through-the-water* velocity is independent of current; its over-the-ground velocity obviously depends upon current, and this dependence becomes more significant in larger currents:

$$\mathbf{x}_{\dot{q}} = \mathbf{x}_{\dot{p}} + \mathbf{x}_{\dot{r}}, \quad (6)$$

where, $\mathbf{x}_{\dot{r}}$ is the relative velocity of the vehicle through the water.

To correct our likelihood formula, we have two options. (1) We can switch from modeling \mathbf{x}_q and $\mathbf{x}_{\dot{q}}$ to modeling \mathbf{x}_r and $\mathbf{x}_{\dot{r}}$, the vehicle kinematics relative to the water column. (2) Alternatively, we can calculate the correct covariance between vehicle over-the-ground velocity and current in order to use the conditional formula, $\Pr(\mathbf{x}_v, \mathbf{x}_c) = \Pr(\mathbf{x}_v|\mathbf{x}_c)\Pr(\mathbf{x}_c)$. Both involve similar mathematical computations.

(i) *Modeling \mathbf{x}_r* In the former variant, we model the vehicle's kinematics relative to the water column. However, if $\mathbf{x}_{\dot{r}}$ represents the vehicle's through-the-water velocity, then \mathbf{x}_r represents the vehicle's position relative to the water. In order to incorporate GPS measurements, we must calculate the true, over the ground position of the vehicle by integrating equation 6. To effect that calculation, we initially let the current velocity field, $x_{\dot{p}}$ vary as a function of depth and time. We integrate equation 6:

$$x_q(T) - x_q(0) = \int_0^T x_{\dot{q}}(t) dt = \int_0^T x_{\dot{r}}(t) + x_{\dot{p}}(s(t), t) dt. \quad (7)$$

We change variables using $\dot{s} = ds/dt$ in the second integral term:

$$= x_r(T) - x_r(0) + \int_{s(0)}^{s(T)} x_{\dot{p}}(s, t(s)) \frac{1}{\dot{s}} ds \quad (8)$$

$$= x_r(T) - x_r(0) + x_p(s(T)) - x_p(s(0)). \quad (9)$$

Here, we recognize $x_p(s)$ as the position of a test particle drifting in the current but changing depths to experience the same currents as the vehicle. The vehicle's over-the-ground position change would then equal the sum of the test particle's position and the vehicle's through-the-water position. Our state vector \mathbf{x}_c now comprises both $\mathbf{x}_{\dot{p}}$ and \mathbf{x}_p .

Practically, the additional current process order manifests as a different \mathbf{G}_c and \mathbf{Q}_c as detailed in Appendix C. In addition to those smoothing terms, the \mathbf{B}_{adcp} and \mathbf{B}_{ttw} matrices adjust to select the proper velocities for their respective measurements. Moreover, the GPS measurement now requires both a \mathbf{B}_{gps}^p and a \mathbf{B}_{gps}^r to add up the true position change of the vehicle.

(ii) *Covariance between $\Pr(\mathbf{x}_v)$ and $\Pr(\mathbf{x}_c)$* If instead we model vehicle kinematics over the ground (as in the basic method), we must derive our maximum likelihood estimate from:

$$\Pr(\mathbf{x}_q, \mathbf{x}_{\dot{q}}, \mathbf{x}_c) = \Pr(\mathbf{x}_q, \mathbf{x}_{\dot{q}} | \mathbf{x}_c) \Pr(\mathbf{x}_c) \quad (10)$$

$$\ell(\mathbf{x}_q, \mathbf{x}_{\dot{q}}, \mathbf{x}_c) = \ell(\mathbf{x}_q, \mathbf{x}_{\dot{q}} | \mathbf{x}_c) + \ell(\mathbf{x}_c). \quad (11)$$

We achieve the conditional likelihood expression by reusing equation 8 to get the joint probability, then conditioning on \mathbf{x}_c . Appendix D provides more details.

d. Optimization and Uncertainty Quantification

The likelihood approach of (5) corresponds to a Bayesian interpretation of the loss. Our prior belief of the Brownian process terms combined with the Gaussian measurement likelihoods results in a combined posterior and its estimator that are Gaussian random variables. Given (5), one can represent the posterior estimator of \mathbf{x} as:

$$\begin{aligned} \hat{\mathbf{x}} = \arg \min_{\mathbf{x}} & \frac{1}{2\sigma_v^2} \|\mathbf{G}_v \mathbf{x}_v\|_{\mathbf{Q}_v^{-1}}^2 + \frac{1}{2\sigma_c^2} \|\mathbf{G}_c \mathbf{x}_c\|_{\mathbf{Q}_c^{-1}}^2 + \\ & \frac{1}{2\sigma_{adcp}^2} \left\| \mathbf{z}_{adcp} - (\mathbf{B}_{adcp}^{\dot{q}} \mathbf{x}_{\dot{q}} - \mathbf{B}_{adcp}^p \mathbf{x}_p) \right\|^2 + \\ & \frac{1}{2\sigma_{ttw}^2} \left\| \mathbf{z}_{ttw} - (\mathbf{B}_{ttw}^{\dot{q}} \mathbf{x}_{\dot{q}} - \mathbf{B}_{ttw}^p \mathbf{x}_p) \right\|^2 + \\ & \frac{1}{2\sigma_{gps}^2} \left\| \mathbf{z}_{gps} - (\mathbf{B}_{gps}^q \mathbf{x}_q - \mathbf{B}_{gps}^p \mathbf{x}_p) \right\|^2. \end{aligned} \quad (12)$$

One can compute the estimator in closed form, using the normal equations. Knowing that any subscript on \mathbf{x} practically represents matrix multiplication and that both \mathbf{Q}^{-1} , as positive definite matrices, factor to LL^T , we can rewrite every term as

$$\frac{1}{2\sigma_i^2} \|\mathbf{A}_i \mathbf{x} - \mathbf{b}_i\|^2. \quad (13)$$

And stacking all \mathbf{A}_i/σ_i into matrix \mathbf{A} and all \mathbf{b}_i/σ_i into vector \mathbf{b} , we can write the optimal value as:

$$\hat{\mathbf{x}} = \mathbf{A} \backslash \mathbf{b} = \mathbf{A}^\dagger \mathbf{b} = (\mathbf{A}^T \mathbf{A})^{-1} \mathbf{A}^T \mathbf{b}. \quad (14)$$

Moreover, the variance of the estimator $\hat{\mathbf{x}}$ has an explicit solution:

$$\text{var}(\hat{\mathbf{x}}) = \mathbb{E}[(\hat{\mathbf{x}} - \mathbf{x})(\hat{\mathbf{x}} - \mathbf{x})^T] = (\mathbf{A}^T \mathbf{A})^{-1}. \quad (15)$$

Here, \mathbb{E} is the expectation operator.

4. Simulation Results

a. Simulation setup

We conducted simulations to compare our method and its variants. Each trial includes a variant with GPS points at both ends of the dive, and an identical variant trial with two GPS points at the beginning and none at the end. This second variant behaves similarly to how Todd et al. (2017) includes initial surface drift velocity, as measured by GPS, as a term in his least-squares solution. However, we leave the observations as positional in nature which allows the Kalman machinery to manage the covariance between positions and velocities. As discussed later in the conclusion, this ability to swap in different measurements shows the flexibility of the probability model framework. Table 1 lists simulation parameters.

b. Parameters and grid-search

While published information about physical devices can inform setting the measurement variance parameters σ^2 , the process variance parameters for smoothing represent prior knowledge of system (vehicle and current) dynamics. We wish to understand how precisely our model's success

Parameter	Value
Duration	3 hrs
Depth	750 m
Hydrodynamic model measurements	500
ADCP measurements	450
ADCP bins	4
ADCP range	12m, upwards-facing
Current	piecewise sinusoid with O(.6) kts
Vehicle TTW velocity	piecewise sinusoid with O(.6) kts
Hydrodynamic model noise	O(1e-2) m/s
ADCP measurement noise	O(1e-2) m/s
GPS measurement noise	O(1) m

TABLE 1: Simulation Parameters, reflecting likely dive of a Seaglider with Nortek ADCP

depends upon knowing the exact process model covariance, a parameter we can only ever assume imprecisely. Thus, in each simulation, we run a parameter search on the covariance coefficients for the process terms, σ_v^2 and σ_c^2 , and evaluate the effect on accuracy metrics.

c. Results

We compare four methods based on different process models: (1) the basic one described in section 3.a, (2) the higher-order one described in section 3.c.1, (3) the process with proper vehicle-current covariance described in section 3.c.2, and (4) a combination of methods 3 and 4: a proper covariance method that smooths to higher order. While section 3.c.2 argues that modeling through-the-water kinematics is mathematically equivalent to modeling true kinematics with appropriate vehicle-current covariance on paper, the higher condition numbers made the former less successful. Thus, we only display results for the latter method. In comparing methods, we use as criteria: (a) The horizontal position accuracy during the dive at optimal process parameters⁷, (b) The current accuracy during the dive at optimal process parameters, (c) The breadth of process parameters that achieve satisfactory results, and (d) performance on simulations including only two closely-placed GPS fixes before the dive and no GPS fix at the end. We evaluate root mean square error (RMSE) across the entire history, averaged over twenty independent trials and displayed in Table 2. Fig. 1 shows the panoply of visualizations produced by each trial, and Appendix E contains the visualizations for each trial, organized for side-to-side comparisons of different trials.

⁷When the process parameters that give rise to the most accurate navigation estimates and those that give rise to the most accurate current estimates disagree, we choose as optimal the parameters that lead to the most accurate current estimation.

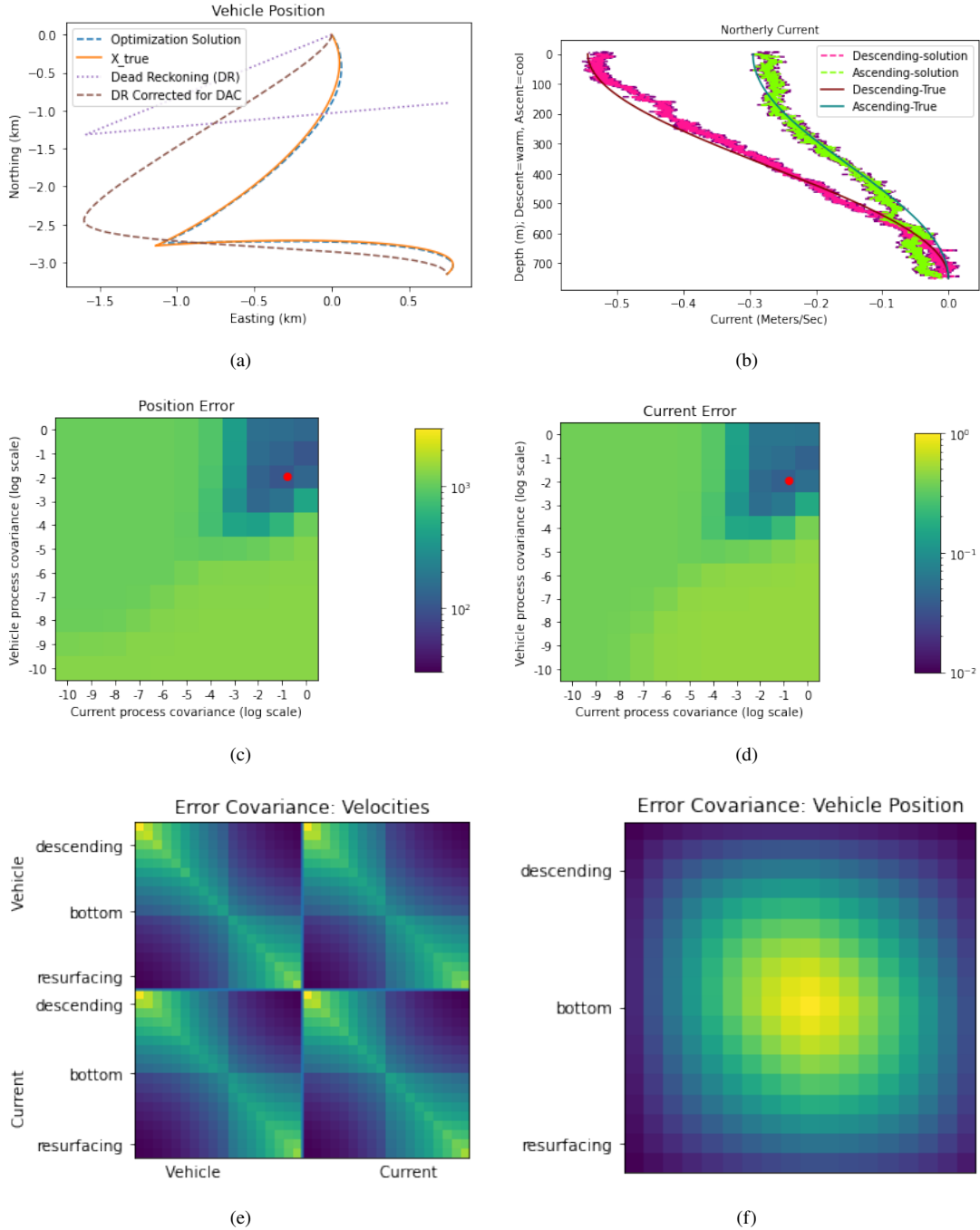


FIG. 1: Visualizations of evaluation criteria for solution method 1 with both starting and ending GPS measurements. (a) Navigation solution, (b) Current solution, (c) Navigation error across process covariance parameter search, with minimizer marked by red dot (d) Current error across process covariance parameter search, with minimizer marked by red dot (e) Vehicle and current velocity estimator uncertainty, and (f) Vehicle position estimator uncertainty. The parameter search plots average twenty simulations. The rest of the plots represent a single simulation from among those twenty. See appendix E for all plots from all trials, organized for comparison across trials.

Method	Variant	Navigation Error	Current Error	Nav err (no final GPS)	Curr err (no final GPS)
1	Basic	102	4.13e-2	380	8.40e-2
2	Higher-order	107	3.83e-2	219	6.09e-2
3	Vehicle-Current covariance	140	5.29e-2	377	8.42e-2
4	Covariance and Higher-order	99.1	3.71e-2	249	6.72e-2

TABLE 2: Results, with the optimal method for each column boldfaced. Navigation RMSE uses units of meters, current RMSE uses units of meters per second. All methods perform competitively, with a different method taking top spot for each metric.

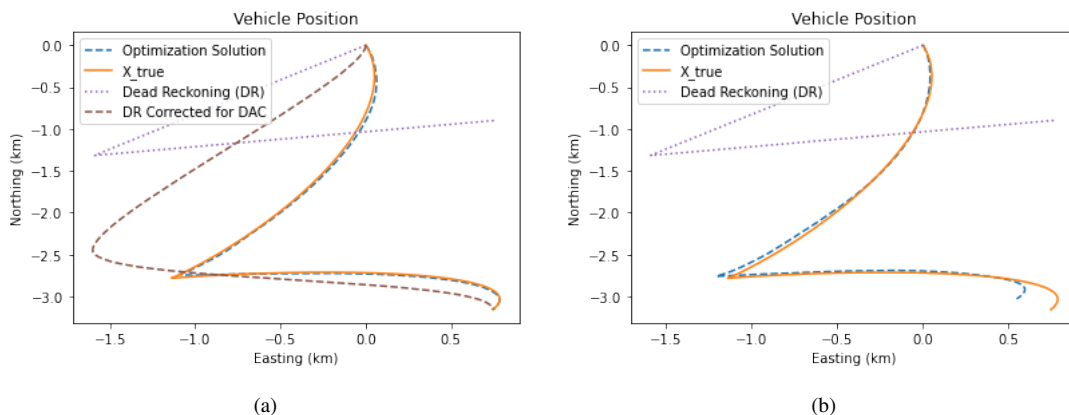


FIG. 2: Navigation error (a) method 1, with start and end GPS points, and (b) method 4, including only starting GPS points. All of this paper’s methods perform well, outperforming DR corrected by DAC and tracking the vehicle to $O(25\text{m/hr})$ before receiving a resurfacing GPS fix.

All solution methods appear to perform adequately, and both higher order methods appear the best at two particular metrics. Considering first navigation error, most methods track the vehicle with at most a 75m difference between true and modeled position. Even with just starting GPS positions, the fourth method keeps track of the vehicle with an accuracy of 100m after four hours. For this particularly challenging track, the level of accuracy displayed in Fig. 2 reflects an impressive success. Looking in more detail at how the choice of vehicle and current process parameters affect navigation error in Fig. 3, we see that the higher order methods (2 and 4) allow a much wider region of parameter space to produce satisfactory results.

As for current error, the higher order methods show a much less noisy solution; Figure 4 illustrates the comparison between methods 3 and 4 for cases including only starting GPS points. The higher-order methods, methods 2 and 4, in the variant without a final GPS point both outperform the other methods and appear visually nicer. Likewise, the much wider acceptable parameter region

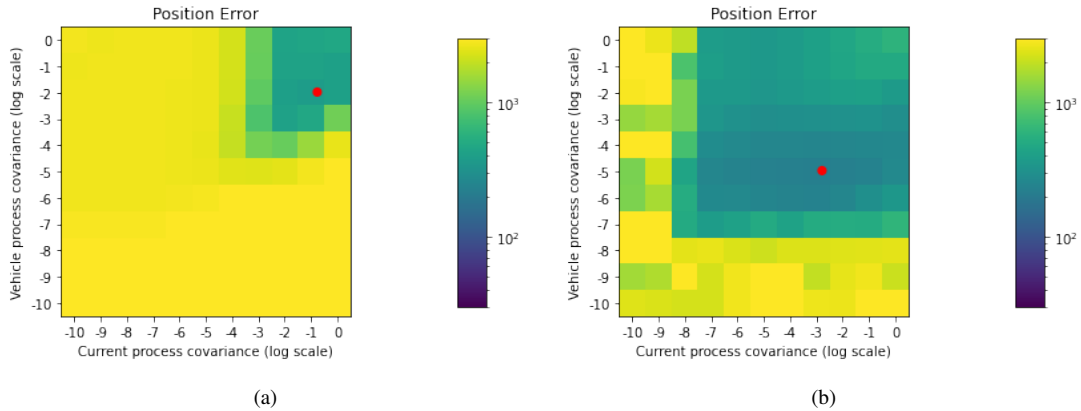


FIG. 3: Navigation error across process covariance parameter search (a) in method 1 and (b) method 2. Both cases shown include only starting GPS points, and the higher-order smoothing methods have a much larger acceptable region of parameter space.

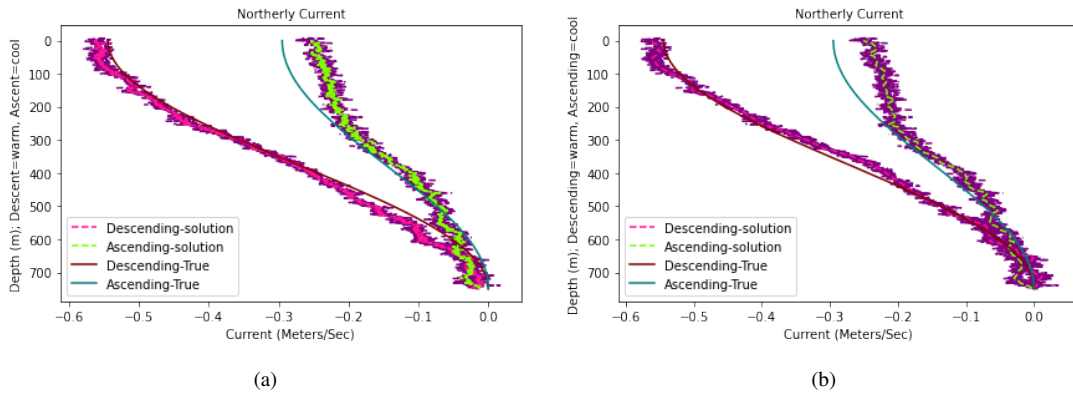


FIG. 4: Current error (a) in method 3 and (b) method 4. Both solutions shown include only starting GPS points. Both the results on prepared metrics and the much smoother profile of the higher order methods recommend methods 2 and 4.

for higher order methods makes them better candidates for a production model. We omit a separate plot for current error across the process covariance parameter search, as it looks similar to Fig. 3.

The estimator variance plots tell several interesting stories. Simulations including only beginning GPS points, such as in Fig. 5, show position and velocity uncertainty growing with duration since the initial GPS observations—as expected. The square-corner covariance plots also appear to exactly replicate those of Brownian motion, providing more confidence that our model performs consistent with assumptions.

Simulations that included both start and finish GPS measurements, as in Fig. 6, predictably show low position uncertainty at the endpoints and high uncertainty at nadir. On the other hand,

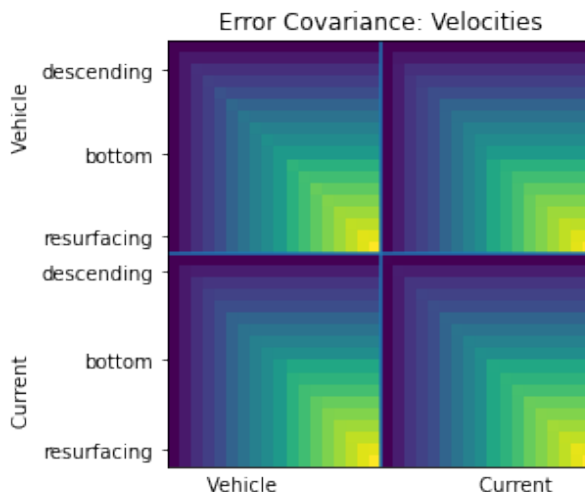


FIG. 5: Method 1 velocity error covariance without a final GPS point appears appropriately similar to the covariance of Brownian motion. Additionally, the repeated off-diagonal terms indicate a lack of identifiability. All methods including only starting GPS points demonstrate these effects.

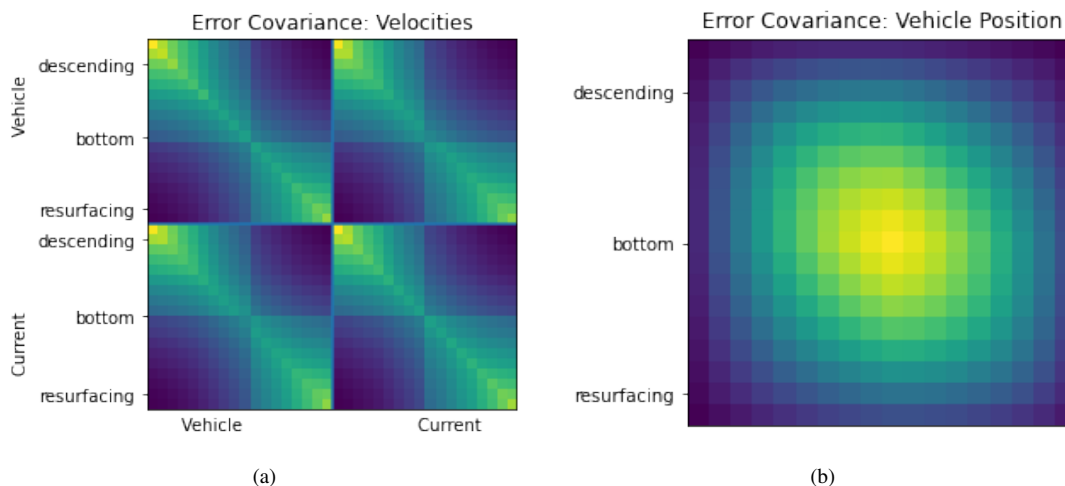


FIG. 6: Method 1 (a) velocity and (b) position estimator error covariance including both starting and ending GPS measurements. This example shows that position uncertainty reaches a minimum in vicinity of GPS observations, while velocity uncertainty reaches a maximum.

velocity uncertainty reaches maxima at the endpoints and a minimum at nadir. Given that GPS measurements affect the integral of velocity, such terms constrain velocities most at the midpoint, where the velocity has the most adjacent points for smoothing. This effect shows that additional measurements reduce uncertainty of the observed quantity, but how that information passes to different process terms depends upon the smoother.

In all cases, the off-diagonal blocks show that vehicle velocity terms correlate highly with their simultaneous currents. Such structure indicates a rank deficiency in our model, a lack of identifiability in whether an individual velocity reflects vehicle motion or currents. It suggests that direct observation of a just a few true vehicle velocities or currents during the dive would dramatically improve estimates. Indeed, Medagoda et al. (2016) finds that such a dramatic correction in navigation estimates occurs as soon as the vehicle gets a DVL lock on the seafloor.

As a final note, while some of our second-order results may appear less smooth than those of other authors', much of that roughness merely reflects the decision not to bin observations.

5. Conclusion and Further Research

We generated data and showed that our basic model, essentially a method of Jonker et al. (2019) without binning, performed reasonably well. Extending the model to higher order to enforce smoothness of velocities improved the model substantially. Our other innovation, the proper covariance relationship between the vehicle process and the current process, yielded only the moral gain of a more rigorous model. All variants significantly outperformed dead reckoning. In particular, models succeeded without the final GPS point as long as two nearby GPS observations before diving helped identify true surface drift.

Various ancillary corrections may help improve the evidence for our major contributions. Most significantly, we may prefer to return to binning observations. Matrix conditioning caused many of the difficulties with higher order models and even with the proper-covariance models. Our time and distance scaling might also prevent the proper-covariance models from showing their merit. Additionally, measurement terms could benefit from reintroducing ADCP bias, compass error, and biofouling errors. Moreover, we have yet to test our model on real data.

As a key avenue for improvement, one could replace the direct matrix inversion of our method with a generic convex solver (which produces equivalent results in the least squares case). The new solver, in turn, would allow for robust vehicle and current processes other than Brownian motion, a topic of interest in Kalman smoothing literature such as Aravkin et al. (2017). Other processes such as an Ornstein-Uhlenbeck process could also help by introducing the assumption that current centers around zero and the vehicle velocity centers around its design drift velocity.

The convex solver would also permit more robust measurement forms than the linear least-squares case. Thus, we could include nonlinear measurements such as range in our framework, as from Ultra-Short Baseline (USBL) or Long Baseline (LBL) systems or even the range-azimuth-elevation of the USBL method in Jakuba et al. (2021). For measurements close to the c_x and c_y , the local coordinates of the sensor, range measurement adds a log likelihood function of:

$$-\ell(\mathbf{z}_{range}|x) = \frac{1}{2\sigma_{range}^2} \|\mathbf{z}_{range}^2 - (\mathbf{B}_{range}^q \mathbf{x}_q - \mathbf{c}_x)^2 - (\mathbf{B}_{range}^q \mathbf{x}_q - \mathbf{c}_y)^2\|^2,$$

where the vector exponents apply elementwise. These measurements, as nonlinear, give rise to a nonconvex likelihood expression. Even so, the expression may still permit finding a good enough local solution, or in cases a global one.

Finally, automatic tuning of process covariance parameters could benefit usability of the model. While we obtained stable results in simulation using grid search for these parameters, a comprehensive approach for simultaneous state and current estimation with more efficient ways of finding underlying variance parameters would more completely solve the engineering problem.

The ability to calculate navigation and current state in real time without external submerged position support allows for more effective use of seagliders. For example, the vehicle could choose to navigate at a depth with beneficial currents to extend its range. It could also dispose of the raw measurements and store the current profile in a compressed form, allowing longer dives and longer deployments. Such innovations would vastly improve the ability to understand global subsurface currents.

APPENDIX A

Kalman Matrices

Referring to time index j for a coordinate x_q^j with velocity $x_{\dot{q}}^j$, the Kalman smoother assumes linear dynamics such that:

$$\begin{aligned} \mathbb{E} \left[x_q^j - x_q^{j-1} | x_q^{j-1} \right] &= 0 \\ \mathbb{E} \left[x_{\dot{q}}^j - x_{\dot{q}}^{j-1} | x_q^{j-1}, x_{\dot{q}}^{j-1} \right] &= \Delta t \cdot x_{\dot{q}}^{j-1}. \end{aligned}$$

As a matrix equation, this expectation takes the form

$$\mathbb{E}[\mathbf{G}_v \mathbf{x}_v] = 0,$$

where

$$\mathbf{G}_v = \begin{bmatrix} -1 & 0 & 1 & 0 & & \\ -\Delta t_1 & -1 & 0 & 1 & & \\ & & -1 & 0 & 1 & 0 \\ & & -\Delta t_2 & -1 & 0 & 1 \\ & & & & \ddots & \ddots \end{bmatrix} \quad \text{and} \quad \mathbf{x}_v = \begin{bmatrix} x_q^1 \\ x_q^1 \\ \vdots \\ x_q^n \\ x_q^n \end{bmatrix}. \quad (\text{A1})$$

The Kalman smoother also assumes that observations are normally distributed and specifies the covariance for each timestep, i.e. $\mathbf{x}_v^j | \mathbf{x}_v^{j-1} \sim \mathcal{N}((\mathbf{G}_v \mathbf{x})^j, \mathbf{Q}_v^j)$, with successive timesteps independent. The overall covariance matrix \mathbf{Q}_v has block diagonals \mathbf{Q}_v^j equal to

$$\begin{bmatrix} \Delta t & \Delta t^2/2 \\ \Delta t^2/2 & \Delta t^3/3 \end{bmatrix}. \quad (\text{A2})$$

This Kalman update and covariance matrix equate to the covariance matrix of a Brownian \mathbf{x}_q when multiplied through the likelihood expression 1.

In \mathbf{x}_c , where the state vector only includes a velocity, one can simply drop the rows/columns of \mathbf{G} and \mathbf{Q} corresponding to position. Finally, since current varies by depth s , we replace Δt with Δs .

APPENDIX B

Higher Order Smoothing

In cases when we include an acceleration term, we can simply integrate the Brownian motion one more time to get \mathbf{G}_v and \mathbf{Q}_v :

$$\mathbf{G}_v = \begin{bmatrix} -1 & 0 & 0 & 1 & 0 & 0 \\ -\Delta t_1 & -1 & 0 & 0 & 1 & 0 \\ -\frac{\Delta t_1^2}{2} & -\Delta t_1 & -1 & 0 & 0 & 1 \\ & & & -1 & 0 & 0 & 1 & 0 & 0 \\ & & & -\Delta t_2 & -1 & 0 & 0 & 1 & 0 \\ & & & -\frac{\Delta t_2^2}{2} & -\Delta t_2 & -1 & 0 & 0 & 1 \\ & & & & & & \ddots & & \end{bmatrix}, \quad \mathbf{Q}_v = \begin{bmatrix} \Delta t & \frac{\Delta t^2}{2} & \frac{\Delta t^3}{6} \\ \frac{\Delta t^2}{2} & \frac{\Delta t^3}{3} & \frac{\Delta t^4}{8} \\ \frac{\Delta t^3}{6} & \frac{\Delta t^4}{8} & \frac{\Delta t^5}{20} \end{bmatrix}. \quad (\text{B1})$$

The current process now has two total orders, and so has similar terms to vehicle smoothing in Appendix A, but again replacing t with s .

APPENDIX C

Modeling Vehicle Relative Velocity

Return to equation 8, where we sought to understand the implication of smoothing x_r , rather than x_q , and recognized x_p terms. If we focus on the second integral,

$$\int_{s(t_1)}^{s(t_2)} x_{\dot{p}}(s, t(s)) \frac{1}{s} ds,$$

we ought to make several assumptions explicit:

1. Current does not change in the time or horizontal strata between observations

2. Depth rate remains constant between two nearby observations.

The first assumptions simplifies our $x_{\dot{p}}$ term, and the second allows the $1/\dot{s}$ becomes a coefficient. Thus, our current process term, equation 2, now uses the process update matrix:

$$\mathbf{G}_c = \begin{bmatrix} -1 & 0 & 1 & 0 & & & \\ -\Delta s_1/\dot{s}_1 & -1 & 0 & 1 & 0 & & \\ 0 & 0 & -1 & 0 & 1 & \ddots & \\ 0 & 0 & -\Delta s_2/\dot{s}_2 & -1 & \ddots & \ddots & \end{bmatrix}, \quad \mathbf{x}_c = \begin{bmatrix} x_{\dot{p}}^1 \\ x_p^1 \\ \vdots \\ x_{\dot{p}}^n \\ x_p^n \end{bmatrix}. \quad (\text{C1})$$

(C2)

Likewise, \mathbf{Q}_c now has blocks:

$$\begin{bmatrix} \Delta s & \Delta s^2/(2\dot{s}) \\ \Delta s^2/(2\dot{s}) & \Delta s^3/(3\dot{s}^2) \end{bmatrix}. \quad (\text{C3})$$

APPENDIX D

Proper Covariance for Current and Vehicle True Velocity

We seek a specification for $\Pr(\mathbf{x}_{\dot{q}}, \mathbf{x}_q | \mathbf{x}_c)$ in equation 10. We first form the correct covariance matrix for $\Pr(\mathbf{x}_{\dot{q}}, \mathbf{x}_q, \mathbf{x}_c)$ and then derive the conditional covariance matrix and expected value. Since \mathbf{G}_v uses the expected value to recenter the process, we need only concern ourselves with a single timestep Δt .

Although we do not utilize an \mathbf{x}_p term, we still return to equation 6. Writing out all the terms as random variables driven by independent Brownian motions W_1^s driving current and W_2^t driving the

vehicle's speed through the water, we calculate:

$$\begin{aligned}
x_c^j - x_c^{j-1} &= \int_{s(t_{j-1})}^{s(t_j)} dW_1^s && \sim \int_0^{\Delta s} dW_1^s \\
x_{\dot{q}}^j - x_{\dot{q}}^{j-1} &= \int_{t_{j-1}}^{t_j} dW_2^t + \int_{s(t_{j-1})}^{s(t_j)} dW_1^s && \sim \int_0^{\Delta t} dW_2^t + \int_0^{\Delta s} dW_1^s \\
x_q^j - x_q^{j-1} &= \int_{t_{j-1}}^{t_j} dt x_{\dot{q}}(t) \\
x_q^j - x_q^{j-1} - \Delta t \cdot x_{\dot{q}}^{j-1} &= \int_{t_{j-1}}^{t_j} dt x_{\dot{q}}(t) - x_{\dot{q}}^{j-1} \\
&= \int_{t_{j-1}}^{t_j} dt \int_{t_{j-1}}^t dW_2^r + \int_{s(t_{j-1})}^{s(t)} dW_1^r && \sim \int_0^{\Delta t} dt \int_0^t dW_2^r + \int_0^{\Delta t} dt \int_0^{s(t)} dW_1^r \\
&= \int_0^{\Delta t} dt \int_0^t dW_2^r + \frac{1}{\dot{s}} \int_0^{\Delta s} ds \int_0^s dW_1^r.
\end{aligned}$$

We have used the independence of successive increments and stationarity to change from $[t_{j-1}, t_j]$ to simpler variables $[0, \Delta t]$. For further simplification, we now let $\Delta x_c = x_c^j - x_c^{j-1}$, $\Delta x_{\dot{q}} = x_{\dot{q}}^j - x_{\dot{q}}^{j-1}$, and $\Delta x_q = x_q^j - x_q^{j-1} - \Delta t \cdot x_{\dot{q}}^{j-1}$. These mean-zero, Gaussian random variables have the covariance matrix:

$$\begin{aligned}
Q &= \begin{bmatrix} \Delta s & \Delta s & \frac{\Delta s^2}{2\dot{s}} \\ \Delta s & \Delta t + \Delta s & \frac{\Delta t^2}{2} + \frac{\Delta s^2}{2\dot{s}} \\ \frac{\Delta s^2}{2\dot{s}} & \frac{\Delta t^2}{2} + \frac{\Delta s^2}{2\dot{s}} & \frac{\Delta t^3}{3} + \frac{\Delta s^3}{3\dot{s}^2} \end{bmatrix} \cdot \begin{bmatrix} \Delta x_c \\ \Delta x_{\dot{q}} \\ \Delta x_q \end{bmatrix} \\
&\quad \Delta x_c \quad \Delta x_{\dot{q}} \quad \Delta x_q
\end{aligned}$$

Marginalizing current and then calculating the conditional distribution gives:

$$\Delta x_c \sim \mathcal{N}(0, \Delta s) \tag{D1}$$

$$\left[\begin{array}{c} \Delta x_{\dot{q}} \\ \Delta x_q \end{array} \right] \Bigg| \Delta x_c \sim \mathcal{N} \left(\left[\begin{array}{c} \Delta x_c \\ \frac{\Delta s}{2\dot{s}} \Delta x_c \end{array} \right], \left[\begin{array}{cc} \Delta t & \frac{\Delta t^2}{2} \\ \frac{\Delta t^2}{2} & \frac{\Delta t^3}{3} + \frac{\Delta s^3}{12\dot{s}^2} \end{array} \right] \right). \tag{D2}$$

When smoothing the vehicle process to higher order and modeling acceleration in this manner, we must also smooth the current process to the same order. Assuming the left side of equation 6 to be smooth would preclude allowing the right side to be non-smooth. Thus, to smooth current

to higher order, we re-notate $x_c(s)$ as $x_{\dot{p}}(s)$, the current velocity, and $x_{\ddot{p}}(s)$, the change in current with depth. The Δ variables (e.g. $\Delta x_q, \Delta x_{\dot{p}}$) then also must adjust to maintain a mean-zero process. The conditional distribution becomes:

$$\begin{bmatrix} \Delta x_{\ddot{q}} \\ \Delta x_{\dot{q}} \\ \Delta x_q \end{bmatrix} \Bigg| \begin{bmatrix} \Delta x_{\ddot{p}} \\ \Delta x_{\dot{p}} \end{bmatrix} \sim \mathcal{N} \left(\begin{bmatrix} \dot{s} \Delta x_{\ddot{p}} \\ \Delta x_{\dot{p}} \\ \frac{\Delta s}{2\dot{s}} \Delta x_{\dot{p}} - \frac{\Delta s^2 \Delta x_{\ddot{p}}}{\dot{s} 12} \end{bmatrix}, \begin{bmatrix} \Delta t & \frac{\Delta t^2}{2} & \frac{\Delta t^3}{6} \\ \frac{\Delta t^2}{2} & \frac{\Delta t^3}{3} & \frac{\Delta t^4}{8} \\ \frac{\Delta t^3}{6} & \frac{\Delta t^4}{8} & \frac{\Delta t^5}{20} + \frac{\Delta s^5}{720 \dot{s}^2} \end{bmatrix} \right). \quad (\text{D3})$$

In both expressions D1 and D3, we roll the conditional mean into our definition of \mathbf{G}_v in order to recover a mean-zero random variable.

APPENDIX E

Complete Plots for Comparison

Acknowledgments. This research was supported by the NOAA Office of Exploration and Research award NA20OAR0110429 and by the Veterans Administration under the GI Bill.

Data availability statement. One can generate the figures and data for this paper by downloading our Python package at <https://github.com/UW-AMO/seaglider-navigation> and running "publish_figures.py". The commit used to generate the exact figures in the paper is 21452bc.

References

- Aravkin, A., J. V. Burke, L. Ljung, A. Lozano, and G. Pillonetto, 2017: Generalized kalman smoothing: Modeling and algorithms. *Automatica*, **86**, 63–86.
- Arnold, S., and L. Medagoda, 2018: Robust model-aided inertial localization for autonomous underwater vehicles. *IEEE conference on Robotics and Automation*, 4889–4896.
- Firing, E., and R. Gordon, 1990: Deep ocean acoustic doppler current profiling. *Proceedings of the IEEE Fourth Working Conference on Current Measurement*, 192–201, <https://doi.org/10.1109/CURM.1990.110905>.
- Jakuba, M. V., J. W. Partan, S. E. Webster, D. Giaya, and C. Ramirez, 2021: Performance of a Low-Power One-Way Travel-Time Inverted Ultra-Short Baseline Navigation System.

- Jonker, J., A. Shcherbina, R. Krishfield, L. Van Uffelen, A. Aravkin, and S. E. Webster, 2019: Preliminary Results in Current Profile Estimation and Doppler-aided Navigation for Autonomous Underwater Gliders. 1–8, <https://doi.org/10.1109/oceanse.2019.8867108>, 1907.02897.
- Liu, X., X. Liu, L. Wang, Y. Huang, and Z. Wang, 2021: SINS/DVL integrated system with current and misalignment estimation for midwater navigation. *IEEE Access*, **9**, 51 332–51 342, <https://doi.org/10.1109/ACCESS.2021.3069469>.
- Medagoda, L., M. V. Jakuba, O. Pizarro, and S. B. Williams, 2010: Water column current profile aided localisation for autonomous underwater vehicles. *OCEANS'10 IEEE Sydney, OCEANSSYD 2010*, 1–10, <https://doi.org/10.1109/OCEANSSYD.2010.5604016>.
- Medagoda, L., and J. C. Kinsey, 2016: Water-Current and IMU Aided AUV Localization in Deep Mid-Water. *IEEE International Conference on Robotics and Automation, (Dvl)*, 2–4.
- Medagoda, L., J. C. Kinsey, and M. Eilders, 2015: Autonomous Underwater Vehicle localization in a spatiotemporally varying water current field. *Proceedings - IEEE International Conference on Robotics and Automation, 2015-June (June)*, 565–572, <https://doi.org/10.1109/ICRA.2015.7139235>.
- Medagoda, L., S. B. Williams, O. Pizarro, and M. V. Jakuba, 2011a: Water column current aided localisation for significant horizontal trajectories with Autonomous Underwater Vehicles. *OCEANS'11 - MTS/IEEE Kona, Program Book*, <https://doi.org/10.23919/oceans.2011.6107240>.
- Medagoda, L., S. B. Williams, O. Pizarro, and M. V. Jakuba, 2011b: Water column current profile aided localisation combined with view-based SLAM for autonomous underwater vehicle navigation. *Proceedings - IEEE International Conference on Robotics and Automation*, 3048–3055, <https://doi.org/10.1109/ICRA.2011.5980141>.
- Medagoda, L., S. B. Williams, O. Pizarro, J. C. Kinsey, and M. V. Jakuba, 2016: Mid-water current aided localization for autonomous underwater vehicles. *Autonomous Robots*, **40 (7)**, 1207–1227, <https://doi.org/10.1007/s10514-016-9547-3>.
- Todd, R. E., D. L. Rudnick, M. R. Mazloff, R. E. Davis, and B. D. Cornuelle, 2011: Poleward flows in the southern California Current System: Glider observations and numerical simulation. *Journal of Geophysical Research: Oceans*, **116 (2)**, 1–16, <https://doi.org/10.1029/2010JC006536>.

Todd, R. E., D. L. Rudnick, J. T. Sherman, W. Brechner Owens, and L. George, 2017: Absolute velocity estimates from autonomous underwater gliders equipped with doppler current profilers. *Journal of Atmospheric and Oceanic Technology*, **34** (2), 309–333, <https://doi.org/10.1175/JTECH-D-16-0156.1>.

Visbeck, M., 2002: Deep velocity profiling using lowered acoustic Doppler current profilers: Bottom track and inverse solutions. *Journal of Atmospheric and Oceanic Technology*, **19** (5), 794–807, [https://doi.org/10.1175/1520-0426\(2002\)019<0794:DVPULA>2.0.CO;2](https://doi.org/10.1175/1520-0426(2002)019<0794:DVPULA>2.0.CO;2).

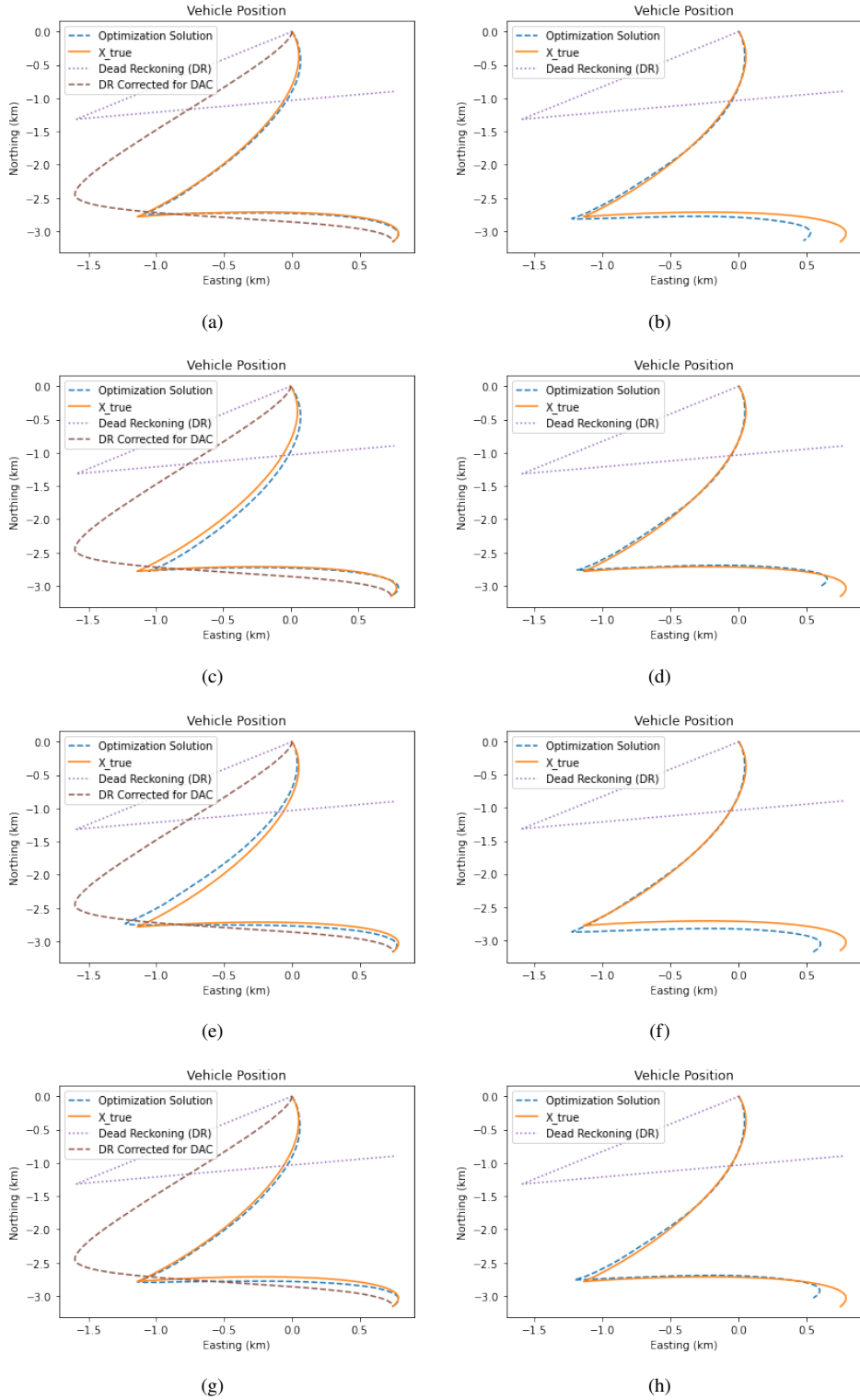


FIG. E1: Representative navigation results from (a, b) method 1, (c, d) method 2, (e, f) method 3, and (g, h) method 4. Trials on the left include start and end GPS points, trials on the right include two starting GPS points only

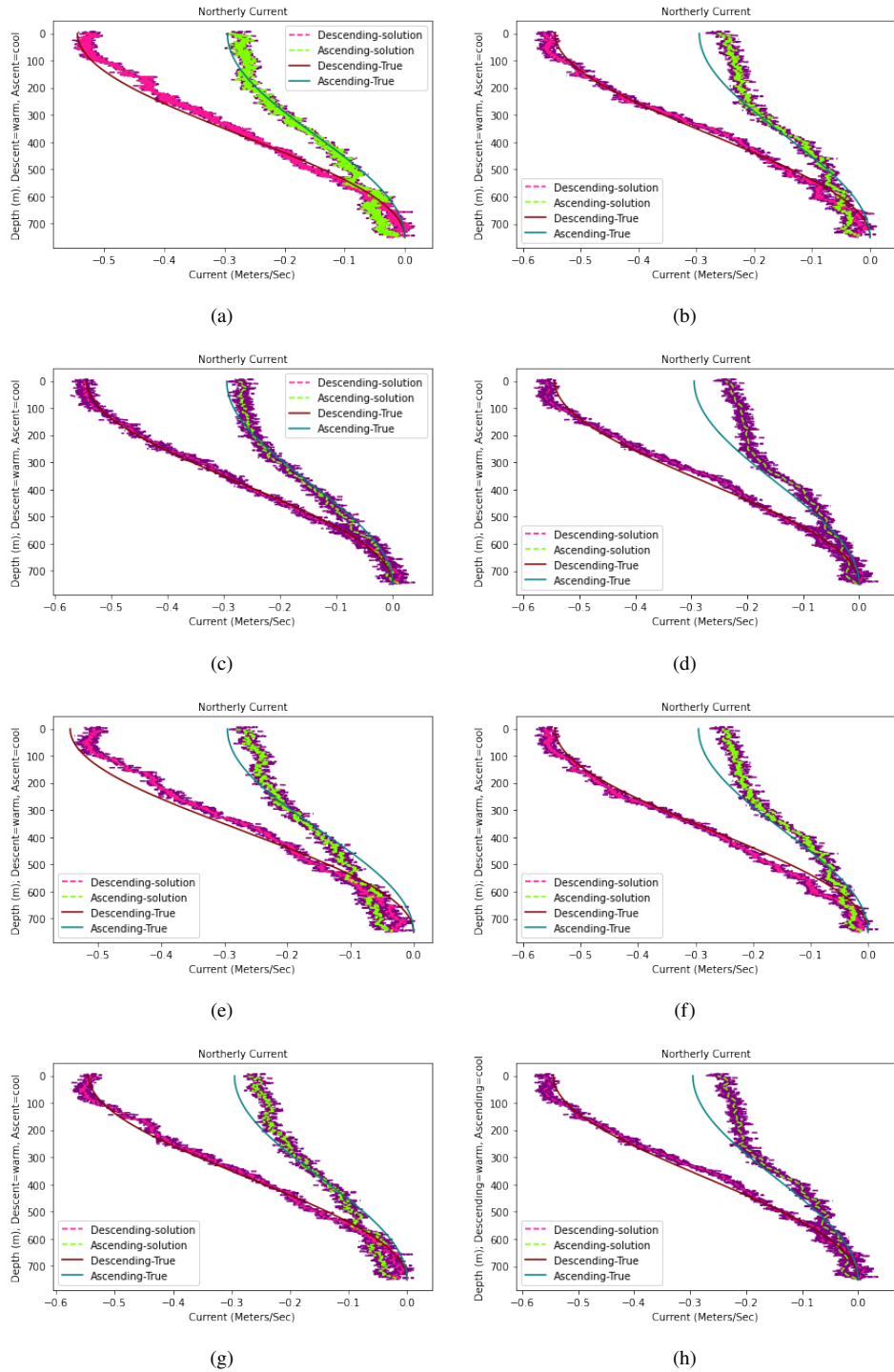


FIG. E2: Representative current results from (a, b) method 1, (c, d) method 2, (e, f) method 3, and (g, h) method 4. Trials on the left include start and end GPS points, trials on the right include two starting GPS points only

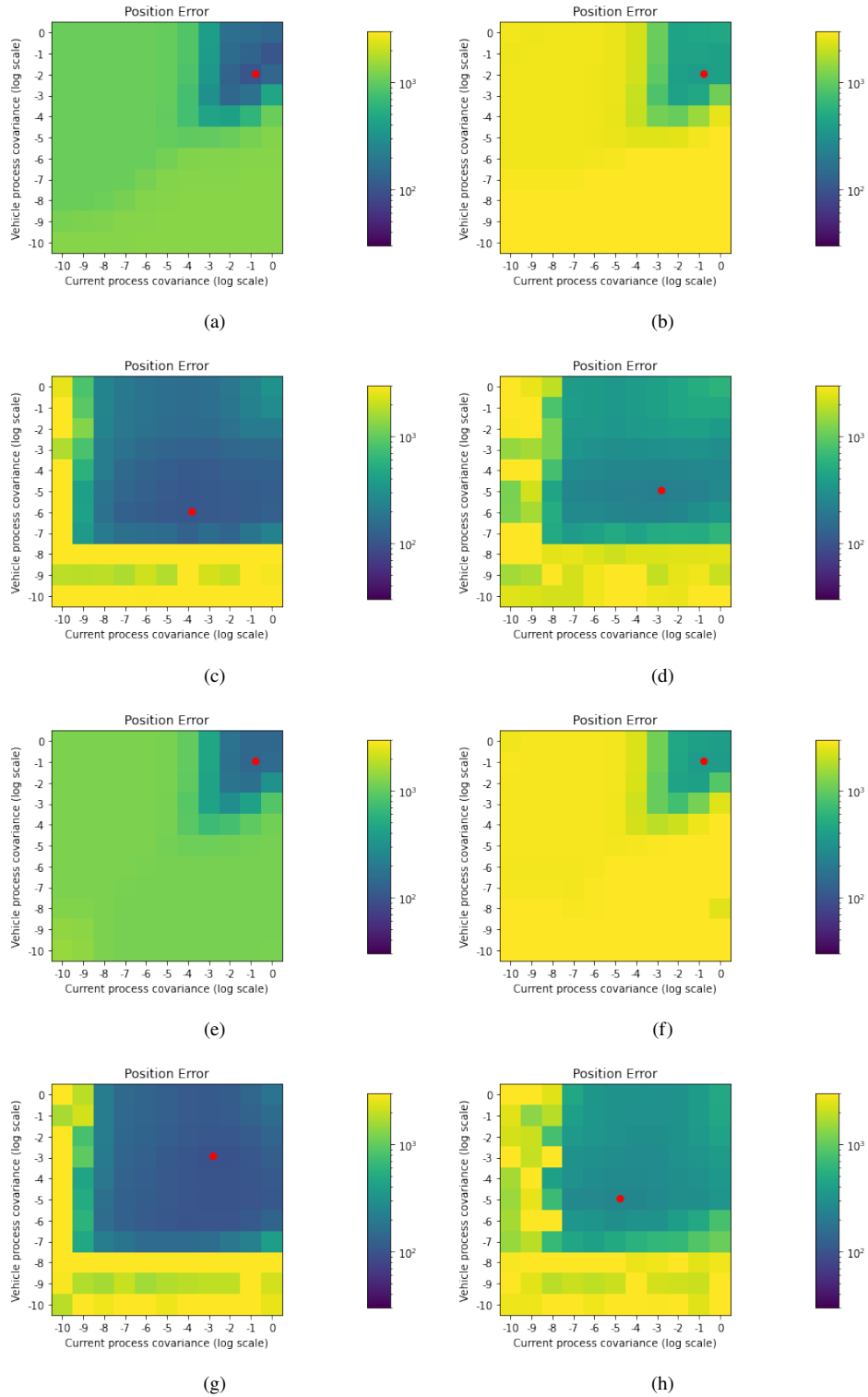


FIG. E3: Navigation parameter search results from (a, b) method 1, (c, d) method 2, (e, f) method 3, and (g, h) method 4. Trials on the left include start and end GPS points, trials on the right include two starting GPS points only. All colors normalized to same values.

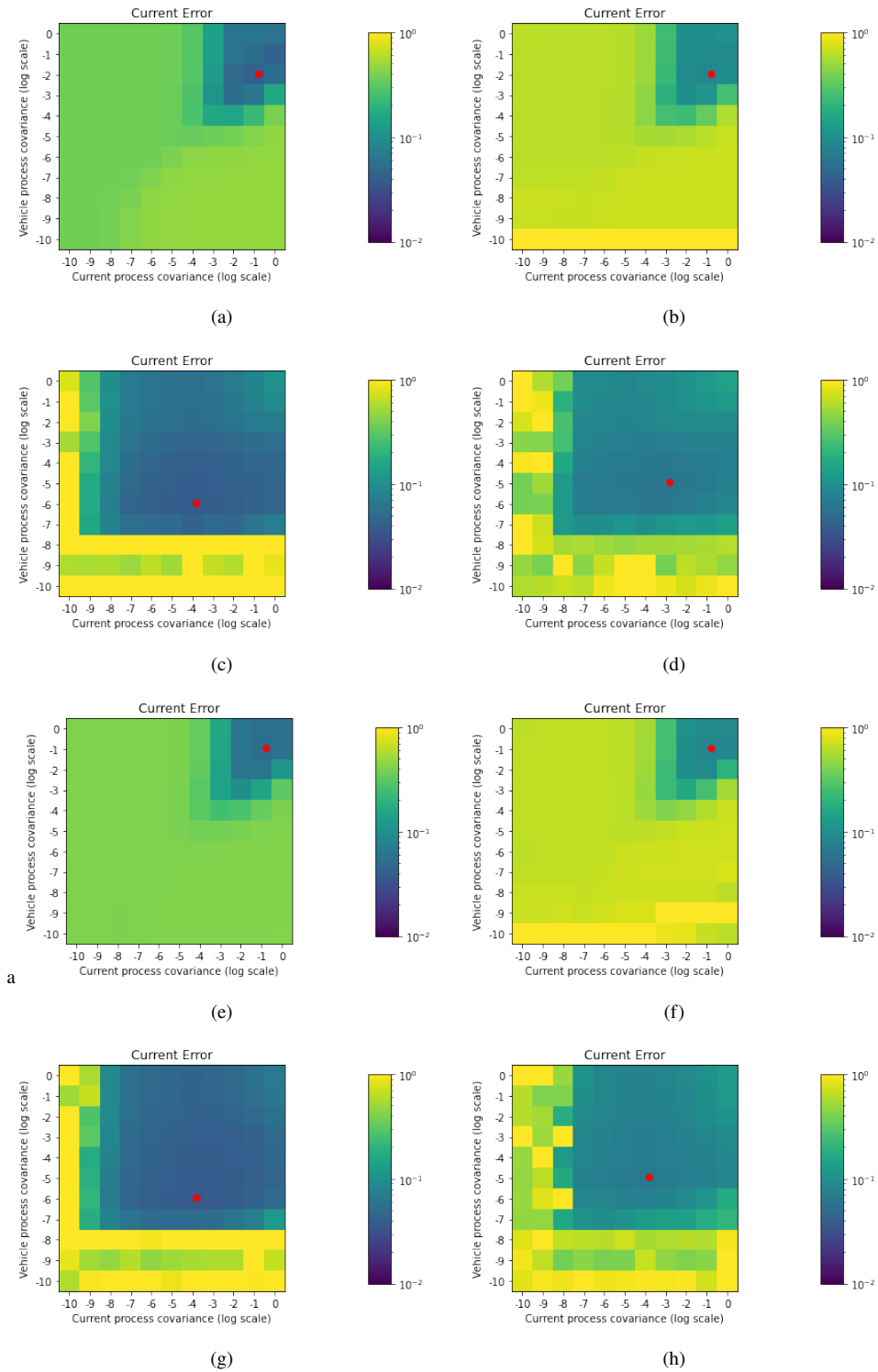


FIG. E4: Current parameter search results from (a, b) method 1, (c, d) method 2, (e, f) method 3, and (g, h) method 4. Trials on the left include start and end GPS points, trials on the right include two starting GPS points only. All colors normalized to same values.

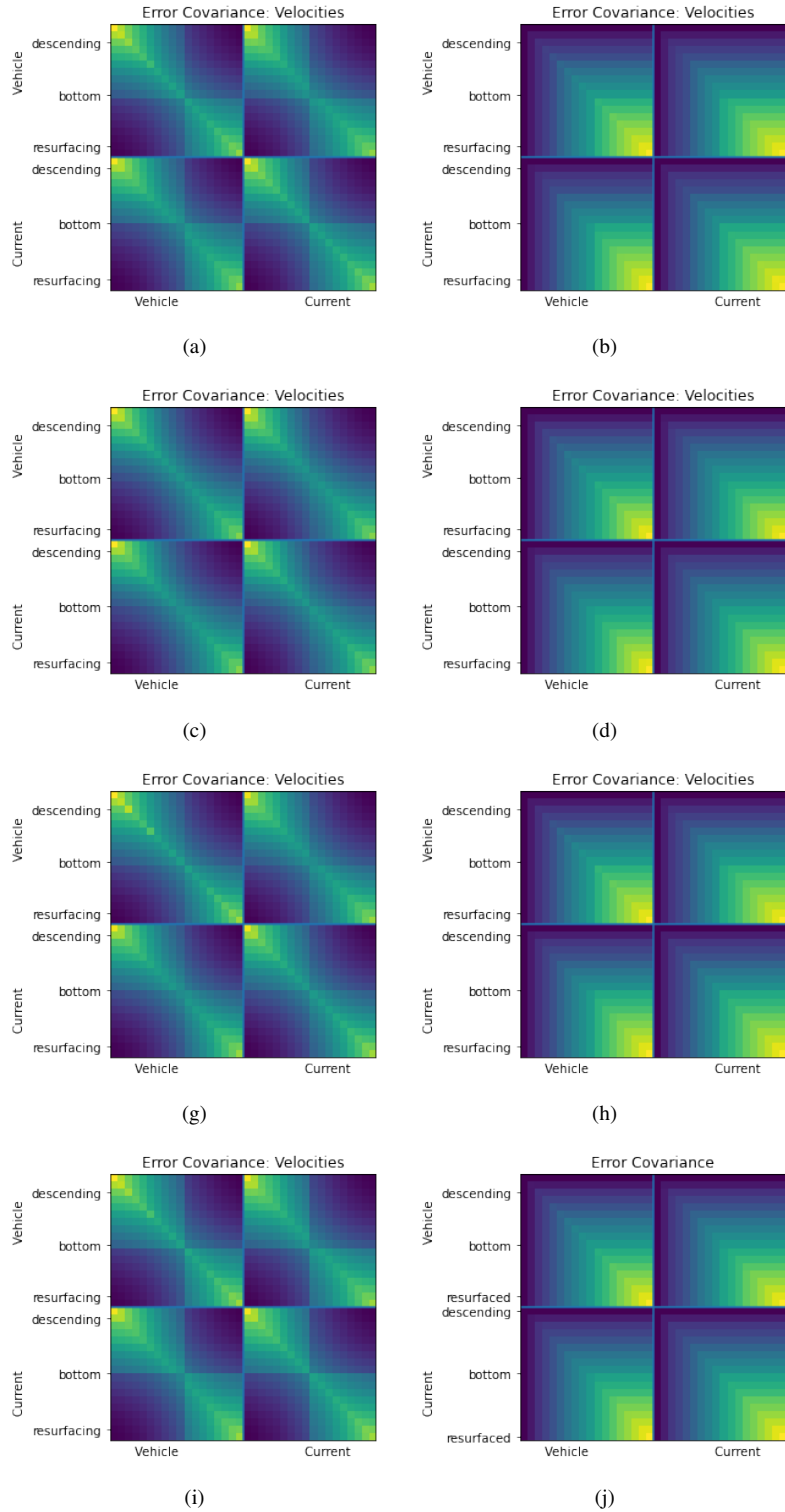


FIG. E5: Velocity estimator covariance (subset of all states) from (a, b) method 1, (c, d) method 2, (e, f) method 3, and (g, h) method 4. Trials on the left include start and end GPS points, trials on the right include two starting GPS points. Colors are **not** normalized to same values.

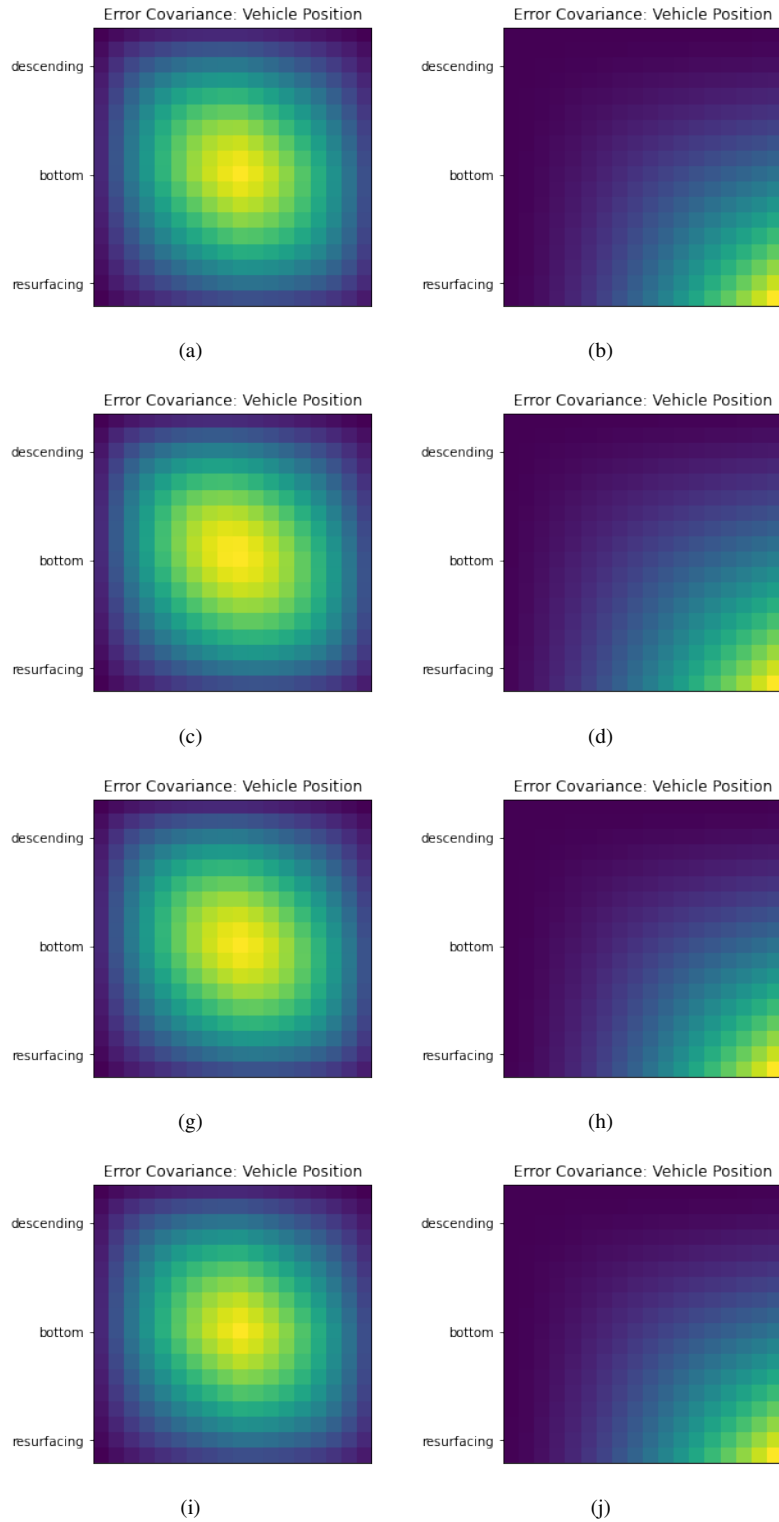


FIG. E6: Navigation position estimator covariance (subset of all states) from (a, b) method 1, (c, d) method 2, (e, f) method 3, and (g, h) method 4. Trials on the left include start and end GPS points, trials on the right include two starting GPS points only. Colors are **not** normalized to same values.